Harmonic Forecasting of Annual Peak Snow Water Equivalent at SNOTEL Monitoring Stations Across the Western United States

Joseph Higginbotham * and John Walker

Posted Date: 7 April 2026

doi: 10.20944/preprints202604.0438.v1

Keywords: snowpack forecasting; SNOTEL; SNOW SENSOR; harmonic analysis; ENSO; snow water equivalent; volcanic forcing; holdout validation

 doi:10.20944/preprints202604.0438.v1

Article

Harmonic Forecasting of Annual Peak Snow Water Equivalent at SNOTEL Monitoring Stations Across the Western United States

Joseph Higginbotham * and John Walker

Walker Water LLC, United States

* Correspondence: joeh@hwh-apps.com

Abstract

We describe a harmonic analysis system for predicting annual peak snow water equivalent (SWE) at SNOTEL monitoring stations operated by the Natural Resources Conservation Service (NRCS) across the western United States. The algorithm, frqsrchX, performs greedy harmonic regression on historical SWE records, identifying persistent periodic climate signals and superimposing volcanic impulse functions to account for episodic radiative forcing from major eruptions. A rigorous five-phase characterization pipeline applies distinct band-limited search strategies per site, and a two-winner selection system identifies optimal configurations by both maximum pass rate and a reliability score that balances accuracy with period stability. Validation uses out-of-sample holdout testing across 15–18 years (2008–2025), graded by an asymmetric scale that penalizes over-prediction more harshly than under-prediction. We report results for 771 SNOTEL and SNOW SENSOR stations across eight western states. Average pass rates range from 88.4% (Montana, 94 sites) to 49.3% (California, 122 sites, including 87 SNOW SENSOR stations). The three commercially targeted states—Colorado (113 sites), Montana (94 sites), and Wyoming (87 sites)—achieve average pass rates of 86.4%, 88.4%, and 84.2% respectively, with 84–90% of sites meeting the ≥80% operational pass-rate threshold using identical universal parameter search procedures and no state-specific tuning. Idaho (85 sites) and Washington (76 sites) show strong intermediate performance at 83.3% and 81.5%. Utah and Oregon show mixed results, while California falls well below operational thresholds. Period stability analysis indicates that 55–62% of qualifying sites in the five strongest states achieve stable signal detection, demonstrating consistent identification of physical climate periodicities. These results demonstrate that periodic climate signals—principally in the ENSO band (2,700–2,900 mY), a mid-range band (~6,000–7,500 mY), and an extended long-period band (10,500–17,000 mY)—carry actionable predictive information about annual peak snowpack at individual station scale.

Keywords: snowpack forecasting; SNOTEL; SNOW SENSOR; harmonic analysis; ENSO; snow water equivalent; volcanic forcing; holdout validation

1. Introduction

Annual peak snowpack, measured as snow water equivalent (SWE), is the dominant driver of warm-season streamflow in the mountainous western United States. Water district managers, reservoir operators, and agricultural planners rely on spring snowpack predictions to make allocation decisions months in advance. Current operational forecasts from the NRCS and the National Weather Service use linear regression of current SWE conditions against historical streamflow relationships, with skill concentrated in the period from February through April when snowpack has partially accumulated. One-year-ahead forecasts—predicting the following year's peak SWE before any snow has fallen—remain an unmet need in operational hydrology.

Harmonic analysis has a long history in geophysical time-series analysis, applied to tides, solar irradiance, and paleoclimate records. The El Niño–Southern Oscillation (ENSO), Pacific Decadal

 doi:10.20944/preprints202604.0438.v1

Oscillation (PDO), Atlantic Multi-decadal Oscillation (AMO), and solar activity cycles all modulate western U.S. precipitation and snowpack on interannual to decadal timescales [7–11]. If these signals are sufficiently periodic and persistent, they should be identifiable in the station-level SWE record and extrapolatable one year forward. The central hypothesis of this work is that greedy harmonic regression, properly constrained against overfitting and augmented with volcanic impulse functions, can extract this predictive signal at individual SNOTEL station scale.

This paper describes the frqsrchX algorithm and its supporting pipeline, reports validation results across 771 stations in eight western states (see Figure 1 for one example and Appendix B for a full report on another site), and characterizes the regional spectral structure that drives performance differences across states. Companion papers establish the physical basis for the methodology: Higginbotham (2026a) examines the role of water vapor and volcanic eruptions in atmospheric radiative forcing; Higginbotham (2026b) validates harmonic analysis over a 350,000-year Antarctic ice core record; Higginbotham (2026c) extends this analysis to CO_2 lag behavior at glacial cycle terminations; and Higginbotham (2025) demonstrates an approach using planetary orbital periodicities applied to sea-level records and emphasizes the importance of proper weighting when combining data sets having different characteristics.

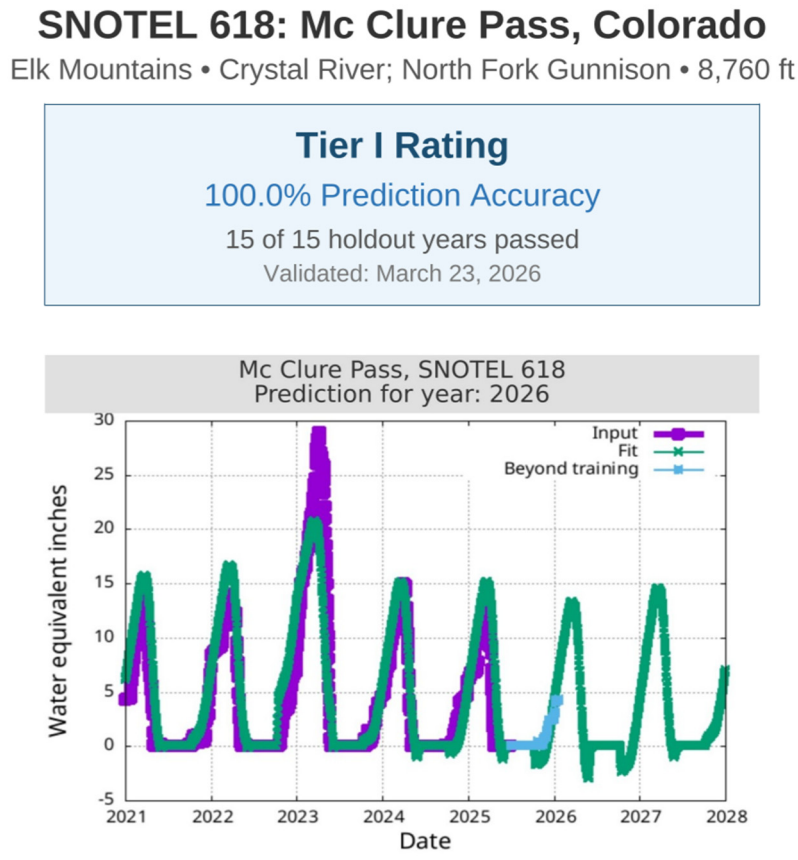

Figure 1. This is an example where fifteen cases of truncated input data successfully predicted peak water equivalent one year beyond. Here the method is applied to predict 2026 peak water equivalent.

2. Data and Methods

2.1. Station Network and Input Data

The NRCS operates the SNOTEL (SNOwpack TELemetry) network of automated monitoring stations across the western United States, with 880 stations in 13 states. A related network of SNOW

 doi:10.20944/preprints202604.0438.v1

SENSOR stations uses different detection equipment (pressure sensing rather than acoustic pillows) but records the same SWE measurement and is included in the NRCS database on the same reporting interface. For California in particular, a substantial fraction of the analyzed sites are SNOW SENSOR stations (87 of 122 analyzed); results for these sites are included in the California totals and are treated as directly comparable to SNOTEL results for the purposes of harmonic prediction. Stations measure SWE, precipitation, air temperature, and other meteorological variables at typical elevations of 6,000–11,000 feet. Records for the longest-running stations extend from the late 1970s to present, providing 38–47 years of annual observations. Stations with fewer than 15 years of record are excluded.

We use daily reported SWE values from the NRCS data site as input to the analysis. While the basic algorithm is a least-squares fit, fit quality is not the attribute used to grade configuration performance. Instead, the fit configuration performance is graded on its ability to predict peak SWE measured a year beyond the truncated input. This is discussed further in the Validation Protocol and Grading section below. We report results for eight states: Colorado (CO), Montana (MT), Wyoming (WY), Idaho (ID), Washington (WA), Utah (UT), Oregon (OR), and California (CA).

2.2. The frqsrchX Algorithm

The frqsrchX algorithm (implemented in Fortran) performs greedy harmonic regression. The model combines two categories of basis functions: (1) volcanic impulse functions, fixed and provided as input parameters, and (2) harmonic functions of the form $A \cdot \sin(2\pi t/P + \varphi)$, where P is the period searched, and A and φ are computed analytically via least-squares once P is determined. The algorithm builds the model incrementally: at each step it searches candidate periods, selects the one most reducing residual variance, tests it against a constraint system, and either accepts or rejects it. Accepted periods are associated with period "slots" to allow comparison of periods across holdout years independent of the order in which they were accepted.

Data preprocessing applies several steps: (1) time conversion to milliYears (mY), where 1,000 mY = 1 year; (2) annual peak SWE extraction from daily records; (3) removal of the mean annual cycle via split-half averaging (see Figure 2); and (4) residual smoothing to reduce high-frequency noise (see Figure 3). No explicit temporal weighting is applied; the algorithm treats all years in the training window with equal weight.

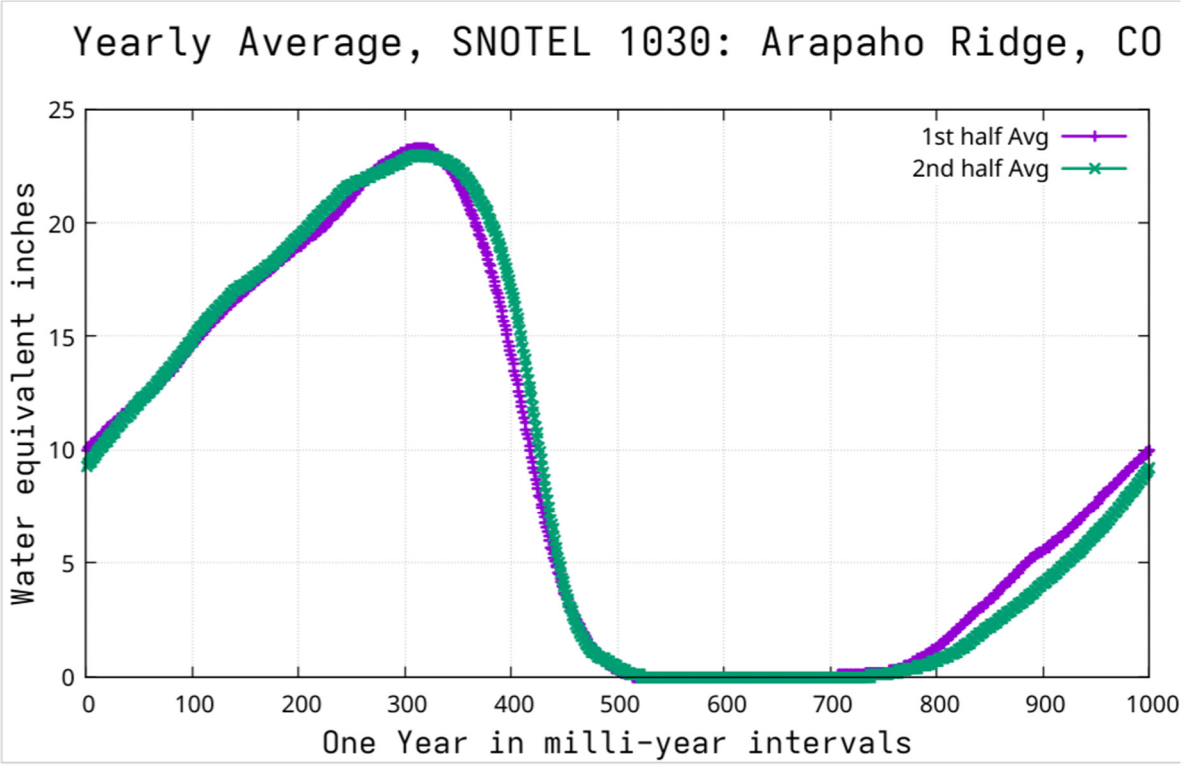

 doi:10.20944/preprints202604.0438.v1

Figure 2. The input data is divided into the early half and late half. These halves are averaged. Then the average for a given year is found by linearly interpolation between these halves.

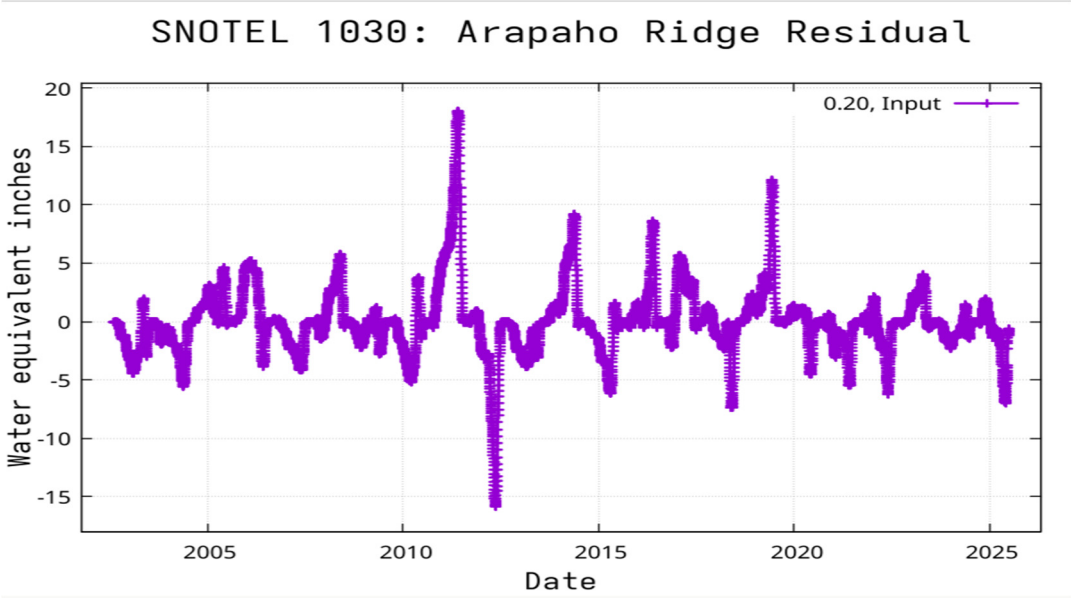

Figure 3. Residual following subtraction of average. The fit is done on this residual and the average is then added back in. Note: the strong peaks and troughs of this figure are NOT at the peak time of year seen in Figure 2. The noisy nature of this residual means that the R^2 is not expected to be high when a limited number of periods are involved in the fit.

2.3. Overfitting Constraint: FNCA

The FNCA (Fractional Normalized Covariance Allowed) constraint prevents overfitting by rejecting candidate periods whose basis functions are insufficiently orthogonal to those already accepted. When a candidate period passes the minimum period separation pre-filter, the algorithm computes two normalized covariance matrices—one measuring geometric overlap between basis functions (Normalized Basis Covariance), one measuring amplitude stability (Normalized Parameter Covariance). If any off-diagonal element involving the candidate exceeds the FNCA threshold in either matrix, the candidate is rejected. This is epistemologically motivated: with approximately 38 years of noisy data, correlated basis functions create an identification problem that cannot be resolved from the record alone. FNCA values tested range from 0.02 (very tight, requiring near-orthogonality) to 0.40 (loose, permitting moderate correlation).

2.4. Band-Limited Search: MASK

The MASK parameter restricts the period search to specified frequency bands for the first MASK_INT period slots. Without MASK constraints, the algorithm can identify spurious high-R^2 periods lacking physical grounding. Bands are derived from spectral peaks of established climate indices (SOI, PDO, AMO, PNA, TSI) and from known solar forcing frequencies. Two specification formats are supported: boundary pairs defining low–high band edges, and center/half-width notation for precision bands.

2.5. Volcanic Forcing Framework

Volcanic eruptions inject aerosols into the stratosphere, reducing solar transmission and causing short-term cooling that manifests in snowpack records as anomalous years unrelated to the periodic climate signal. Without volcanic impulse functions, the algorithm attempts to fit these step changes with sinusoids, corrupting period selection. Four volcanic transfer functions are used in production: (V1) Hunga Tonga stratospheric water vapor injection (peak 2023.0, exponential decay); (V2) 2018

 doi:10.20944/preprints202604.0438.v1

warm snow drought impulse (center 2017.5); (V3) Pinatubo fast component (center 1991.8); and (V4) Pinatubo slow component (center 1991.4). The physical basis for volcanic impulse modeling is established in Higginbotham (2026a). An independent validation of the impulse framework—applying 23 eruption impulses and 15 periodic functions to 60 years of atmospheric transmission data—achieves $R^2 = 0.94$ (see Figure 4), demonstrating that the parameterization captures real stratospheric aerosol physics with high fidelity (Walker Water LLC, internal technical report, 2026).

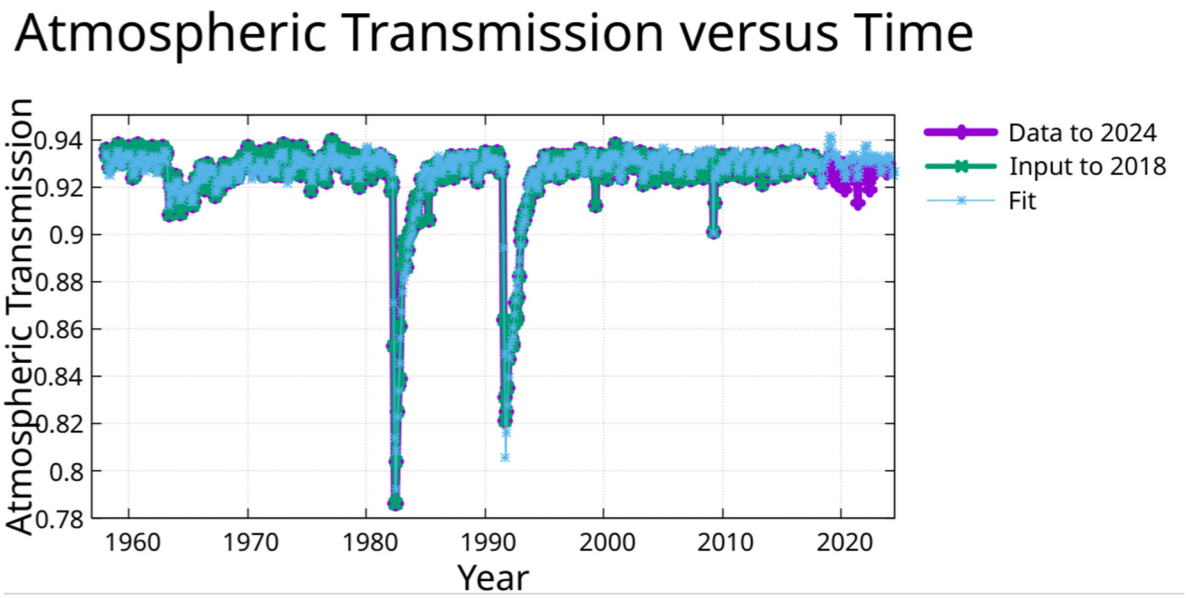

Figure 4. Here Atmospheric Transmission is fit using a constant, fifteen periods, and 23 impulse functions for volcanic eruptions.

2.6. Five-Phase Characterization Pipeline

Each station is characterized through five independent phases, each employing a distinct search strategy: Phase A (OPEN) applies no MASK constraints, providing an unconstrained baseline; Phase B (Mod_000) uses three broad bands covering the ENSO band (2,700–2,900 mY), a mid-range band (~6,000–7,500 mY), and an extended long-period band (10,500–17,000 mY); Phase C (Mod_00C) applies 35 narrow precision bands (1% half-width) derived from climate index spectral peaks; Phase D (Mod_00D) uses minimal two-band constraints covering only the ENSO and extended long-period bands; and Phase E (Mod_00E) applies 10 broad bands providing full-spectrum coverage. All phases test the same configuration order: 1p/0.40, 2p/0.20, 2p/0.10, 2p/0.05, 2p/0.02, 3p/0.20, 3p/0.10, 3p/0.05, 4p/0.20, 4p/0.10, 4p/0.05, where np denotes the number of harmonic periods and the decimal denotes the FNCA threshold.

2.7. Validation Protocol and Grading

Holdout validation tests 15 graded years, grading the prediction one year beyond the holdout year (2009–2026, excluding plot-only years 2018, 2023, and 2026). For each holdout year, all data from June of that year forward is removed and the algorithm predicts the following year's peak SWE using only the prior data. This simulates the real-world condition in which the forecast is made mid-season before any snow has fallen in the target year. Grading uses an asymmetric scale: over-prediction is penalized more harshly than under-prediction because shortfall destroys client trust and creates operational emergencies. A grade of C− or better constitutes a pass. The tier system is: Tier I (≥85% pass rate, high reliability), Tier II (≥75%, acceptable), and Tier III (<75%, below operational threshold). The reliability score is computed as $(1 - VCV^2) \times PassRate$, where VCV is the slot-based coefficient of variation across holdout year period selections, measuring consistency of period identification across

 doi:10.20944/preprints202604.0438.v1

the validation window. The full grading scale is given in Appendix A and Appendix B shows a full report for SNOTEL site 1030 which includes plots of holdout year analysis with grades given below.

2.8. Period Stability Metric (VCV)

Period stability (VCV) is computed from the slot-based period distribution across holdouts. Each holdout's periods are assigned to frequency slots; adjacent slots are merged if their combined coefficient of variation is below 5%; slots appearing in more than 50% of mature holdouts are considered dominant. Per dominant slot, instability is the maximum of: the within-slot coefficient of variation; and (1 − √occupancy). VCV is the worst instability across dominant slots. Only holdouts with training data span ≥15 years contribute to VCV, excluding early holdouts that cannot resolve long-period signals. Stability categories: STBL (VCV < 0.10, consistent signal detection), MDRT (0.10–0.30, moderate variation), USTBL (≥0.30, scattered or unreliable periods).

3. Results

3.1. Overview Across Eight States

We report results for 771 SNOTEL and SNOW SENSOR stations across eight western states. Table 1 summarizes performance by state. Average pass rates span from 88.4% (Montana) to 49.3% (California), with a clear geographic gradient from interior mountain states to Pacific maritime states. All five inland states (CO, MT, WY, ID, WA) achieve average pass rates above 80%, while the three Pacific-influenced states (UT, OR, CA) fall at or below 75%. The *inland* state of Washington is included with the others by neglecting the Cascades' maritime west slope and focusing on performance characteristics. The system achieves 85%+ average pass rates across the three primary states, decisively rejecting the no-skill null hypothesis. Under the null (each holdout a coin flip, $p = 0.5$), the probability that any single site passes 14 or more of 15 holdout years by chance alone is approximately $P \approx 0.00049$, and the probability of achieving the observed three-state average pass rates simultaneously across 294 independent sites is effectively zero.

Table 1. Validation performance summary by state.

State	Sites	Avg Pass Rate	Tier I	Tier II	Tier III	≥80% Sites
Colorado	113	86.4%	71%	15%	14%	84%
Montana	94	88.4%	77%	14%	10%	90%
Wyoming	87	84.2%	60%	28%	13%	87%
Idaho	85	83.3%	54%	27%	19%	81%
Washington	76	81.5%	59%	8%	33%	66%
Utah	112	75.5%	29%	26%	46%	51%
Oregon	82	70.8%	21%	12%	67%	33%
California	122	49.3%	2%	1%	98%	3%

Tier I ≥85% pass rate; Tier II ≥75%; Tier III <75%. ≥80% = operational threshold. California total of 122 includes 87 SNOW SENSOR and 35 SNOTEL stations.

3.2. Primary Validation States: Colorado, Montana, Wyoming

Colorado (113 sites), Montana (94 sites), and Wyoming (87 sites) form the primary validation group. All three states were characterized using the same universal parameter search—identical

 doi:10.20944/preprints202604.0438.v1

MASK band definitions, FNCA thresholds, and configuration order—with no state-specific tuning whatsoever. Colorado shows 71% Tier I, 15% Tier II, and 14% Tier III sites. Montana is the strongest performer with 77% Tier I and 90% of sites meeting the ≥80% pass-rate operational threshold. Wyoming shows 60% Tier I with a higher Tier II fraction (28%), suggesting more sites near the 75–85% boundary rather than true failure. The consistent ~13% Tier III rate across all three states is notable: it appears to represent an irreducible fraction of sites where the periodic climate signal is too weak relative to local noise—weather, terrain, or land use—to support reliable prediction. The uniformity of this fraction across states, despite their distinct climates, supports the interpretation that it reflects a fundamental limit of the periodic signal approach rather than a tuning deficiency.

3.3. Secondary States: Idaho and Washington

Idaho (85 sites) and Washington (76 sites) extend the validated range into neighboring states, again using the universal parameter search. Idaho (83.3% average, 81% of sites ≥80%) performs comparably to the primary three states, suggesting similar interior continental climate dynamics. Washington (81.5% average) shows stronger Tier III representation (33%), likely reflecting the mixed Pacific maritime and continental climate of the Cascades. Sites on the maritime-influenced western slopes of the Cascades may experience more stochastic precipitation patterns less amenable to harmonic prediction.

3.4. Lower-Performing States: Utah, Oregon, California

Utah (112 sites, 75.5% average) and Oregon (82 sites, 70.8% average) show mixed performance using the same universal parameters. Utah's large Tier III fraction (46%) and low ≥80% rate (51%) may reflect the influence of the Great Basin's moisture sources, which are more sensitive to atmospheric river events and less driven by persistent ENSO-linked teleconnections. Oregon's predominantly maritime climate produces a 67% Tier III rate, indicating that harmonic prediction is not broadly applicable in that state with the current universal parameter set. California (122 sites: 35 SNOTEL and 87 SNOW SENSOR, 49.3% average) is effectively non-viable under the current approach: 98% Tier III, with only 3% of sites meeting the ≥80% threshold. The SNOW SENSOR sites in California perform comparably to—and in aggregate slightly below—the SNOTEL sites in the same state. California's highly variable precipitation, dominated by atmospheric rivers and North American monsoon interactions, appears insufficiently periodic for harmonic prediction at the site level regardless of sensor type.

3.5. Period Stability Analysis

Table 2 shows period stability distributions by state. Among the five strongest states, 55–62% of sites achieve STBL (VCV < 0.10), indicating consistent identification of the same physical period across holdout year windows. USTBL rates (VCV ≥ 0.30, indicating scattered period selection) are low in Wyoming (7%), Idaho (9%), Montana and Colorado (both 13%), and Washington (28%). The lower-performing states show higher USTBL rates: Utah 29%, Oregon 30%, California 40%. The STBL/USTBL distinction matters for operational forecasting: STBL sites provide high-confidence predictions because the same climate signal is consistently identified across holdout years; USTBL sites may achieve acceptable pass rates by fitting different signals in different holdout windows, providing less assurance for future years outside the validation set.

Table 2. Period stability distributions by state.

State	STBL (VCV<0.10)	MDRT (0.10–0.30)	USTBL (≥0.30)
Colorado	58%	28%	13%
Montana	59%	27%	13%

 doi:10.20944/preprints202604.0438.v1

Wyoming	62%	31%	7%
Idaho	55%	35%	9%
Washington	41%	32%	28%
Utah	42%	25%	29%
Oregon	56%	13%	30%
California	23%	37%	40%

STBL: VCV<0.10 (consistent detection); MDRT: 0.10–0.30 (moderate variation); USTBL: ≥0.30 (scattered).

3.6. Period Complexity and Regional Spectral Structure

Period complexity distributions reveal distinct regional spectral signatures. Colorado favors simple models: 28% of winning configurations use a single period and 42% use two periods, reflecting strong ENSO coupling. Montana has the richest multi-period structure, with the highest 4p fraction (24%), consistent with a broader spectral signature involving a shifted long-period band (approximately 14,000–17,000 mY, possibly PDO-related rather than solar). Wyoming is the most balanced across complexity levels, with the highest 3p fraction (32%). These differences emerge from the identical universal parameter search across all states, confirming that the spectral structure differences are properties of the climate signal rather than artifacts of parameter choices.

Table 3. Period complexity of winning configurations (primary states).

State	1-Period	2-Period	3-Period	4-Period
Colorado	27.7%	41.6%	14.2%	12.9%
Montana	18.9%	36.9%	20.5%	23.6%
Wyoming	15.6%	35.5%	31.7%	17.2%

Percentages of sites whose winning configuration uses each period count. Remaining fraction uses higher period counts.

3.7. Phase Win Distribution

Phase D (minimal two-band MASK: ENSO + extended long-period) is the most frequent score-gated winner across all three primary states. Its tight constraint on two physically motivated bands forces rock-solid period selection in those bands while leaving remaining slots to search freely, producing the highest reliability scores even when pass rates are marginally lower than more complex configurations. This finding is consistent with the bias-variance tradeoff: the tighter constraint reduces variance (period stability improves) at the cost of minor bias (slightly lower mean pass rate), but the net reliability score is higher because the VCV penalty is reduced more than the pass rate is reduced. Across all three primary states, more than 90% of qualifying sites show the same configuration as both the pass-rate winner and the score-gated winner.

4. Discussion

4.1. Why Harmonic Analysis Works for Mountain Snowpack

The success of harmonic analysis at individual SNOTEL stations challenges the common assumption that station-scale snowpack variability is dominated by unpredictable weather noise. Our results indicate that periodic climate signals—primarily ENSO-band oscillations (period approximately 2.8 years), a mid-range signal (~7 years), and a long-period cycle (10.5–17 years, likely

 doi:10.20944/preprints202604.0438.v1

solar or PDO related)—carry sufficient predictive power to achieve operational pass rates at 80–90% of interior mountain station sites. The same greedy harmonic framework recovers canonical Milankovitch periods in the 350,000-year ice core record [2,3] and accounts for 94% of variance in six decades of atmospheric transmission data, suggesting that the approach captures genuine periodic physics rather than fitting noise.

4.2. Geographic Gradient in Performance

The geographic gradient in performance follows a logical pattern. Interior continental sites experience winter precipitation predominantly from Pacific storm tracks modified by the jet stream, itself strongly modulated by ENSO [10,11]. This teleconnection is persistent and periodic, making it detectable and extrapolatable. Pacific maritime sites, by contrast, receive a larger fraction of precipitation from atmospheric rivers—narrow filaments of moisture-laden air that are episodic rather than periodic—reducing the signal-to-noise ratio for harmonic methods [12]. California's poor performance is consistent with its known precipitation volatility: a single atmospheric river event can deliver more water than an entire average wet season, and the occurrence of such events is not well predicted by interannual climate indices.

4.3. The Over-Prediction Problem

Over-prediction failures constitute 83–96% of all grading failures across states. This systematic bias reflects a known limitation: the algorithm identifies the frequency of ENSO-driven drought patterns but cannot predict their amplitude. An extreme La Niña, producing anomalously deep snowpack, is predicted as a La Niña year but the magnitude may be underestimated; an extreme El Niño drought is predicted correctly in sign but the model over-predicts the magnitude. The Hunga Tonga (2022) eruption added a potentially confounding forcing: its unprecedented injection of water vapor into the stratosphere [1] may have caused systematic over-prediction in 2023–2025 if the decay function used to represent this in the model is too long.

4.4. Universal Parameters vs. State-Specific Tuning

The universal parameter search approach—identical Mod files for all sites in all states—is both a strength and a limitation. Its strength is that it eliminates state-specific overfitting and demonstrates true generalizability. Its limitation is that state-specific or site-specific tuning could improve performance for the current Tier III sites. Montana's long-period band, centered near 14,000–17,000 mY rather than the Colorado/Wyoming 10,500–12,500 mY, suggests that state-level MASK adjustments might yield incremental improvement in that state. Site-specific modifier files (Mod_NNN) are supported by the pipeline infrastructure and represent a potential premium service tier.

4.5. Prospective Validation: 2026 Season

The 2026 prediction season constitutes the first real-time out-of-sample test of this system. Forecasts have been generated for approximately 294 sites in Colorado, Montana, and Wyoming. When 2026 peak SWE observations become available (typically April–May), they will provide the first prospective validation—predictions made before the season, evaluated against actual outcomes. This will also clarify whether the pass-rate winner or the reliability score-gated winner is the better predictor of future performance.

4.6. Geographic Predictors of Performance

An internal analysis of site-level geographic and pattern-stability characteristics [13] conducted when only three states had been analyzed concluded that *pattern stability* — defined as consistency of the annual SWE cycle shape and amplitude between early and late halves of the station record — is a stronger predictor of forecasting success than any individual geographic factor. The eight-state

 doi:10.20944/preprints202604.0438.v1

dataset substantially extends and refines that finding. Examining pass rates of sites with stable period detection (STBL, VCV < 0.10) across states reveals a hierarchy that is unmistakably geographic but operates through two distinct mechanisms. In the four interior continental states, STBL sites average 83–90% pass rates, comfortably in the Tier I range. Washington's STBL sites average 88.6%, essentially matching the interior states — Washington's performance deficit arises not from failure of STBL sites but from a higher fraction of sites (28%) classified as USTBL, concentrated on the maritime-influenced western slopes of the Cascades where atmospheric river precipitation creates unstable period detection. This distinction is practically important: Washington has two performance populations rather than one degraded one, and the eastern-slope and interior sites perform as well as Colorado.

The Pacific maritime states reveal a second, more fundamental mechanism. Oregon's STBL sites average only 75.5%, barely at the Tier II threshold, and 45% of Oregon's Tier III sites are STBL — meaning that a stable, consistently detected periodic signal does not translate into forecasting skill. The periodic ENSO and long-period signals are present and identifiable, but their predictive amplitude is too small relative to the stochastic variance introduced by episodic Pacific storm systems and orographic precipitation to dominate the holdout-year outcome. California represents the limiting case: STBL, MDRT, and USTBL sites all average approximately 47–50% pass rates, with period stability carrying no predictive information whatsoever. At this point, stochastic atmospheric river events so thoroughly dominate the annual SWE variance that the harmonic model captures only noise, regardless of how consistently the algorithm identifies periodic structure in the training data. This distinction — between geographic settings where periodic signals are detectable but weak (Oregon) and settings where they are irrelevant (California) — is not visible from geographic factors alone and was not resolvable from the 15-site pilot study.

Utah occupies an intermediate position consistent with the Great Basin's mixed climate regime. Utah's STBL sites average 79%, above Oregon's but below the interior states, with 36% of STBL sites falling into Tier III. Two specific geographic effects compound the state-wide average. First, Great Salt Lake-generated precipitation introduces stochastic lake-effect variability at sites within 50 miles of the lake, precisely the mechanism the pilot analysis identified for the Promontory and Snowbird sites. Second, the Great Basin's more diffuse and variable moisture sourcing weakens the ENSO teleconnection that drives predictability in the Rockies, reducing the amplitude of the periodic signal even at sites with favorable elevation and pattern stability.

Regional spectral structure also carries geographic fingerprints. Colorado and Wyoming sites most frequently identify a long-period signal in the 10,500–12,500 mY band, consistent with a known solar-activity cycle influencing continental precipitation. Montana sites instead concentrate that long-period energy near 14,000–17,000 mY, shifted toward periods associated with the Pacific Decadal Oscillation. Montana's higher latitude and stronger oceanic coupling likely explain this shift. The practical consequence — that Montana achieves the highest average pass rate (88.4%) despite this spectral difference — confirms that the harmonic approach is capturing real physical signals in both cases rather than artifacts of the search strategy. Taken together, these geographic patterns suggest a predictability hierarchy governed primarily by the ratio of periodic climate forcing amplitude to stochastic precipitation variance: highest in ENSO-coupled interior mountain ranges, degraded by lake-effect noise and mixed moisture sources in the Great Basin, reduced by weak ENSO teleconnection amplitude in Pacific maritime settings, and effectively zero where episodic atmospheric rivers dominate.

5. Conclusions

We have demonstrated that greedy harmonic regression with FNCA overfitting constraints and volcanic impulse functions provides skillful one-year-ahead predictions of peak annual SWE at individual SNOTEL and SNOW SENSOR stations across the western United States. Performance is strongest in interior continental states (Montana, Colorado, Wyoming, Idaho) where ENSO teleconnections produce persistent periodic signals in snowpack records. The system uses universal parameter searching without any state-specific tuning, achieving 84–90% of sites meeting the ≥80%

 doi:10.20944/preprints202604.0438.v1

operational threshold in the three primary states. Period stability analysis confirms that for the majority of high-performing sites, the same physical climate periodicities are consistently identified across holdout years, providing mechanistic confidence in the forecasts beyond pure statistical pattern-matching. California (122 sites), Oregon, and Utah show progressively lower performance consistent with increasing maritime influence and precipitation volatility; California's SNOW SENSOR sites perform similarly to its SNOTEL sites in this regard. Future work will address ENSO amplitude supplementation using Southern Oscillation Index scaling, optimization of the Hunga Tonga decay function, and systematic evaluation of site-specific configuration tuning for Tier III sites.

Data Availability: SNOTEL and SNOW SENSOR data are publicly available from the NRCS Report Generator at https://wcc.sc.egov.usda.gov/reportGenerator/. Station characterization results and site-level validation summaries are available from Walker Water LLC on request. The frqsrchX Fortran source code and pipeline scripts are proprietary to Walker Water LLC.

Acknowledgments: The authors thank the NRCS for maintaining the SNOTEL and SNOW SENSOR networks and providing open access to station data. The characterization pipeline runs on Linux workstations at the Walker Water field site in western Colorado.

We thank James D. Clippard, PhD Geophysics, for interesting discussions and advice.

Conflict of Interest: Walker Water LLC has a commercial interest in deploying the described forecasting system. All validation results are generated by automated software from out-of-sample holdout data without human intervention.

Appendix A: Prediction Grading Scale

Predictions are graded on an academic scale based on the ratio of predicted peak SWE to observed peak SWE, expressed as a percentage. A ratio of 100% indicates a perfect prediction. Over-prediction (ratio > 100%) is penalized more harshly than under-prediction because shortage destroys client trust and creates operational emergencies for water managers. Over-prediction enters the failing range at +27% deviation; under-prediction fails at −31% deviation. A grade of C− or better constitutes a pass. Grading is performed entirely by software with no human intervention.

Table A1. Full Asymmetric Grading Scale.

Grade	Over-Prediction (pred/obs)	Under-Prediction (pred/obs)	Result
A+	100–102%	97–99%	Pass
A	103–105%	94–96%	Pass
A−	106–108%	90–93%	Pass
B+	109–111%	87–89%	Pass
B	112–114%	84–86%	Pass
B−	115–117%	80–83%	Pass
C+	118–120%	77–79%	Pass
C	121–123%	74–76%	Pass
C−	124–126%	70–73%	Pass (threshold)
D+	127–129%	67–69%	Fail
D	130–132%	64–66%	Fail

 doi:10.20944/preprints202604.0438.v1

D−	133–135%	60–63%	Fail
F	≥136%	<60%	Fail

Over-prediction enters failing range at +27% deviation; under-prediction fails at −31% deviation.

Appendix B: Example Site Report — SNOTEL 1030 Arapaho Ridge, Colorado

To illustrate the validation process and output format, this appendix reproduces key sections from the formal site characterization report for SNOTEL 1030 (Arapaho Ridge, Colorado), a Tier I site in the Never Summer Mountains, Grand County, Colorado.

Snowpack Forecasting

Site Characterization Report

SNOTEL 1030: Arapaho Ridge, Colorado

Never Summer Mountains • Colorado River Headwaters; Willow Creek • 10,960 ft

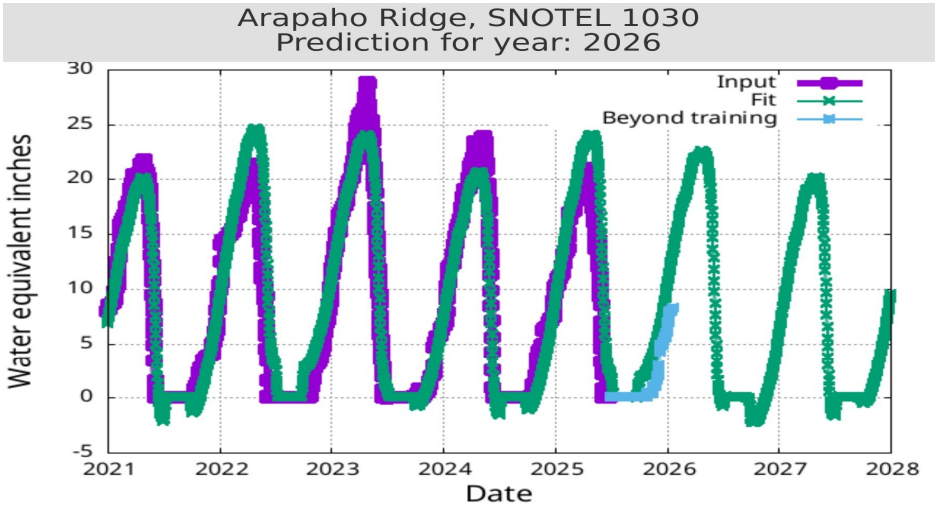

Figure B1. Purple: observed SWE. Green: model fit and extrapolation. Blue: measured data beyond training cutoff.

Tier ratings are based on objective evaluation of prediction of omitted data, measured later in time than input training data. Grading of predictions is done by software without human intervention. This information is provided to assist the responsible purchasing party in making decisions.

Site Overview

SNOTEL station 1030 at Arapaho Ridge sits at 10,960 ft in Grand County, Colorado. The station has recorded continuous snowpack data since 2002, providing over two decades of snow water equivalent (SWE) measurements for analysis.

Snowmelt from the Arapaho Ridge area contributes to both the Colorado River Headwaters and Willow Creek. This positions the station's snowpack data as relevant to water supply planning for downstream communities dependent on spring runoff from the Never Summer Mountains. Arapaho Ridge is one of 113 SNOTEL stations across Colorado characterized by Walker Water's automated pipeline.

 doi:10.20944/preprints202604.0438.v1

Station Name	Arapaho Ridge
SNOTEL Number	1030
Elevation	10,960 ft (3,340 m)
Location	40°21′N, 106°22′W
County	Grand County, Colorado
HUC Basin	Rabbit Ears Creek–Troublesome Creek
Data Record	2002–present
Operating Agency	NRCS

Validation Results: Arapaho Ridge

Arapaho Ridge achieves a **93.3% pass rate** across 15 graded holdout years (2009–2025, excluding plot-only years), earning a **Tier I** rating. One failure occurs across the record: prediction year 2012 (F). Two additional years (2018 and 2023) are tested as plot-only predictions but are excluded from the pass rate calculation because they correspond to known anomalous forcings that fall outside the system's prediction scope.

Signal analysis indicates **high** consistency in the underlying climate signals detected at this site, with a **reliability score of 92.6 out of 100**. The reliability score reflects both prediction accuracy and the consistency of the detected climate patterns across different evaluation windows. Higher scores indicate greater confidence in future predictions.

Grade Distribution

Table B1. Grade distribution across 15 holdout years, Arapaho Ridge.

Grade Range	A+/A/A−	B+/B/B−	C+/C/C−	D+/D/D−	F
Count	6	4	4	0	1
Result	Pass	Pass	Pass	Fail	Fail

A+/A/A− = excellent; B+/B/B− = good; C+/C/C− = adequate pass; D and F = fail.

The grade distribution shows 14 of 15 holdout predictions at C− or better. A+ grades at 2015 and 2017 demonstrate the system's ability to produce near-exact predictions. The model shows particular strength in the later record, with 11 consecutive passing grades from 2013 through 2025.

Year-By-Year Results

Table B2. Year-by-year holdout prediction grades, Arapaho Ridge.

Year	Grade	Status	Year	Grade	Status
2009	A−	Pass	2018	P*	Plot-only
2010	B	Pass	2019	B+	Pass
2011	C−	Pass	2020	A−	Pass
2012	F	Fail	2021	A−	Pass

 doi:10.20944/preprints202604.0438.v1

2013	A	Pass	2022	C−	Pass
2014	C+	Pass	2023	P*	Plot-only
2015	A+	Pass	2024	B	Pass
2016	B−	Pass	2025	C−	Pass
2017	A+	Pass	2026	?	Unknown

* Plot-only (P) years are tested but excluded from the pass rate. 2018: warm snow drought (La Niña coinciding with anomalous warmth). 2023: Hunga Tonga eruption forcing period.

Holdout Prediction Plots

The following figures show each holdout prediction in context. In each plot, the purple curve is observed SWE data, the green curve is the model's fit to the training data and extrapolation, and the blue curve is the measured data beyond the training cutoff. The grade beneath each plot indicates how accurately the extrapolation matched the observed peak SWE in the holdout year. Two grades are shown: the first is the one-year-ahead grade (used for pass/fail), the second is the two-year-ahead grade (informational only).

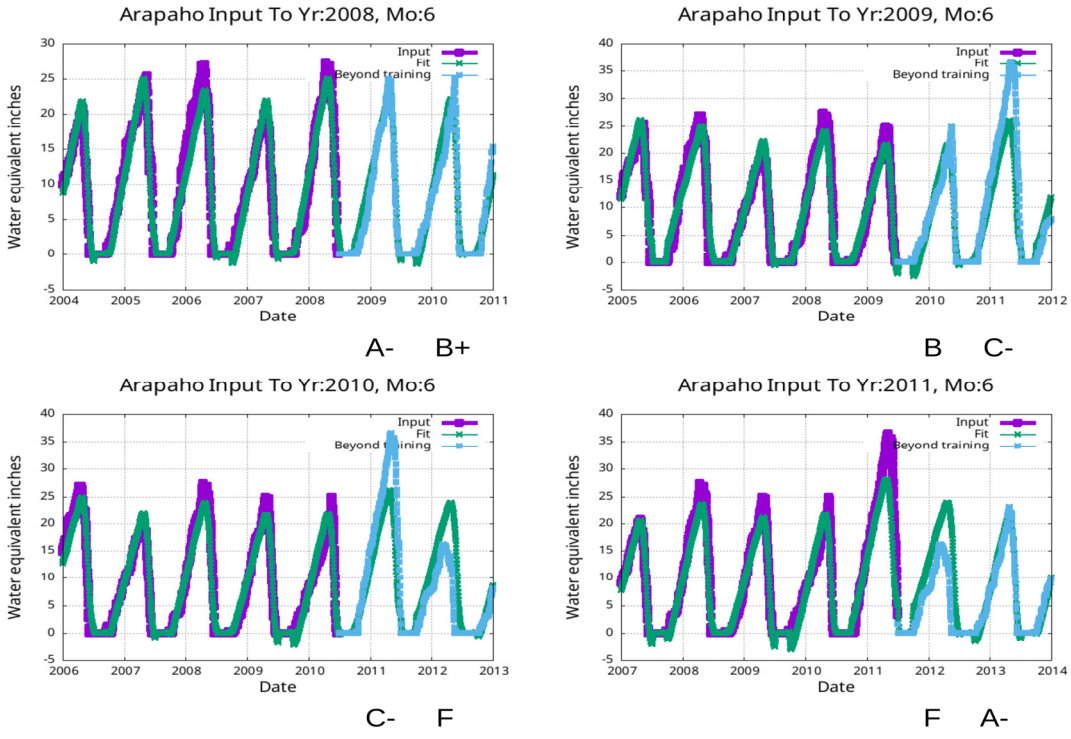

Figure B2. Holdout predictions for 2009-2012. The A- at 2009 is a passing grade. The B at 2010 is a passing grade. The C- at 2011 is a passing grade. The F at 2012 is a failure.

Preprints.org (www.preprints.org) | NOT PEER-REVIEWED | Posted: 7 April 2026 doi:10.20944/preprints202604.0438.v1

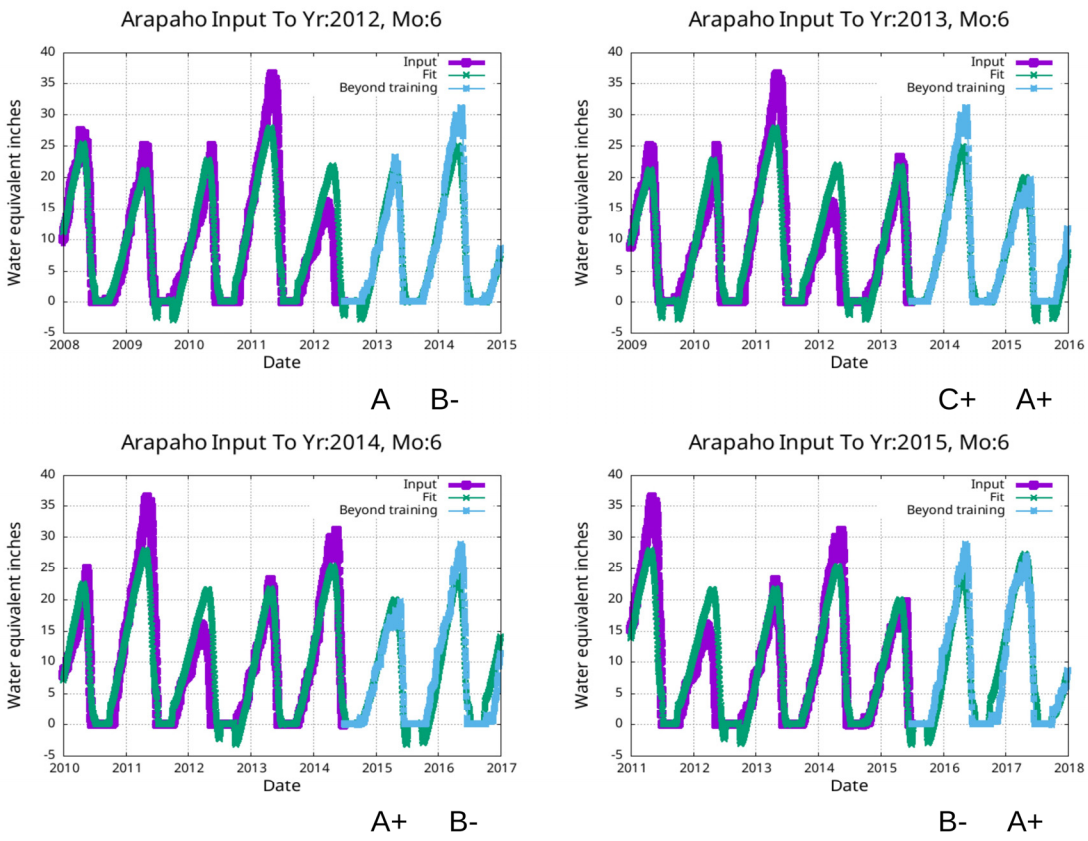

Figure B3. Holdout predictions for 2013–2016. The A at 2013 is a passing grade. The C+ at 2014 is a passing grade. The A+ at 2015 is a passing grade. The B– at 2016 is a passing grade.

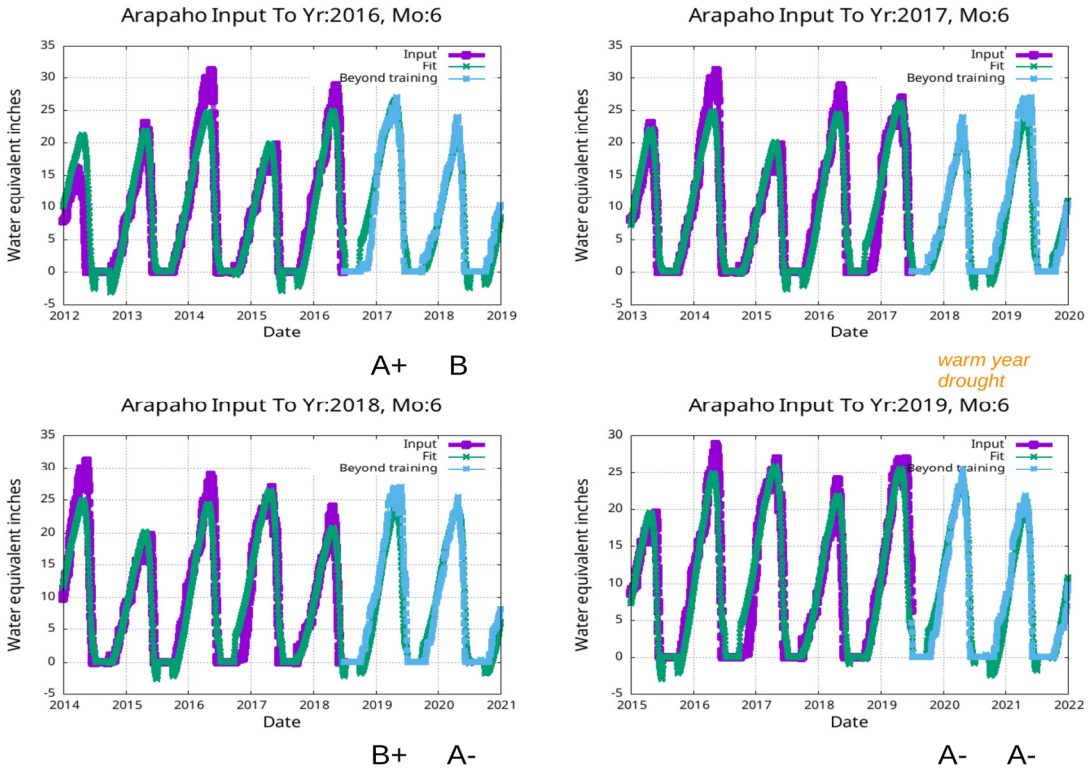

Figure B4. Holdout predictions for 2017–2020. The A+ at 2017 is a passing grade. The 2018 prediction (warm snow drought year) is tested as plot-only. The B+ at 2019 is a passing grade. The A– at 2020 is a passing grade.

 doi:10.20944/preprints202604.0438.v1

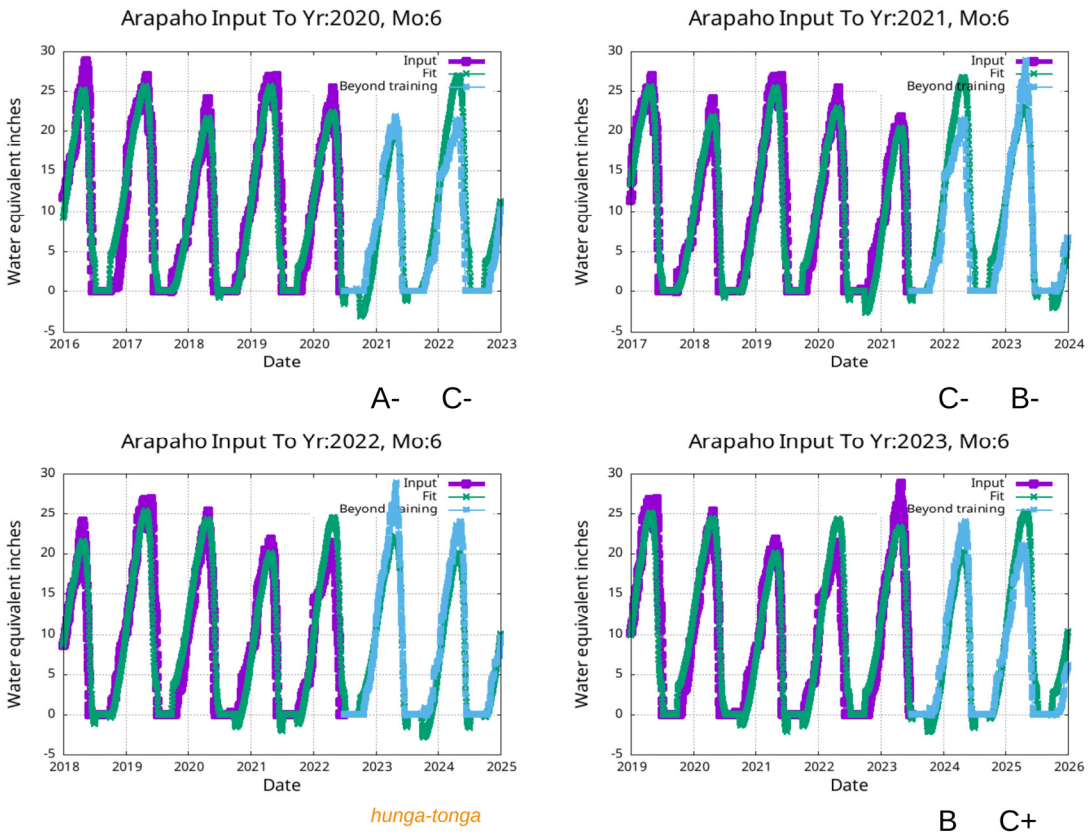

Figure B5. Holdout predictions for 2021–2024. The A– at 2021 is a passing grade. The C– at 2022 is a passing grade. The 2023 prediction (Hunga Tonga eruption) is tested as plot-only. The B at 2024 is a passing grade.

2026 Season Prediction

The 2026 prediction (see Figure B1, and Figure B6 - Right) represents the system's operational forecast. Unlike the holdout tests, this prediction uses the complete training record and is being validated in real time as the snow season progresses. The NRCS station data shown earlier (TBD of median as of March 23, 2026) provides early-season context, though peak SWE typically occurs in April–May at this elevation.

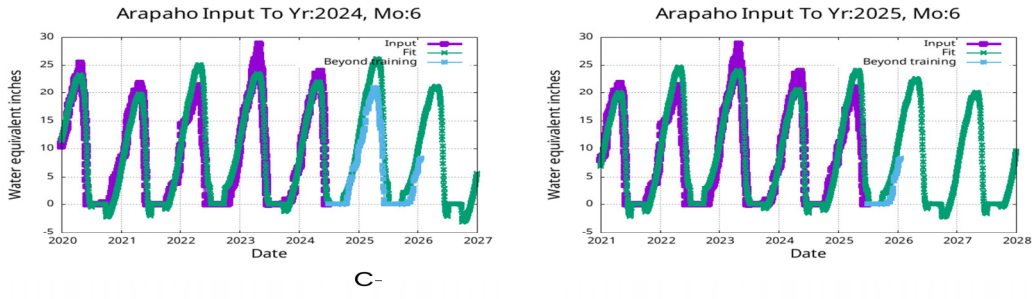

Figure B6. Left: final holdout at 2025 (grade C–, pass). Right: 2026 prediction using all available training data through mid-2025. The green extrapolation curve shows the model's forecast for peak SWE in the 2025–2026 snow season.

The 2026 prediction will be validated against observed peak SWE when the 2025–2026 snow season concludes.

 doi:10.20944/preprints202604.0438.v1

Arapaho Ridge is one of 113 SNOTEL stations across Colorado characterized by Walker Water's automated pipeline. The statewide results demonstrate that the harmonic forecasting approach works systematically, not just at hand-picked favorable sites.

Northern Colorado stations (above 39.5°N latitude) average 88.7% pass rates, while the full Colorado network averages approximately 80%. Geographic patterns are informative: sites at lower elevations and higher latitudes tend to have cleaner periodic signals, likely because their snowpack variability is more strongly coupled to regional-scale climate oscillations rather than local topographic effects.

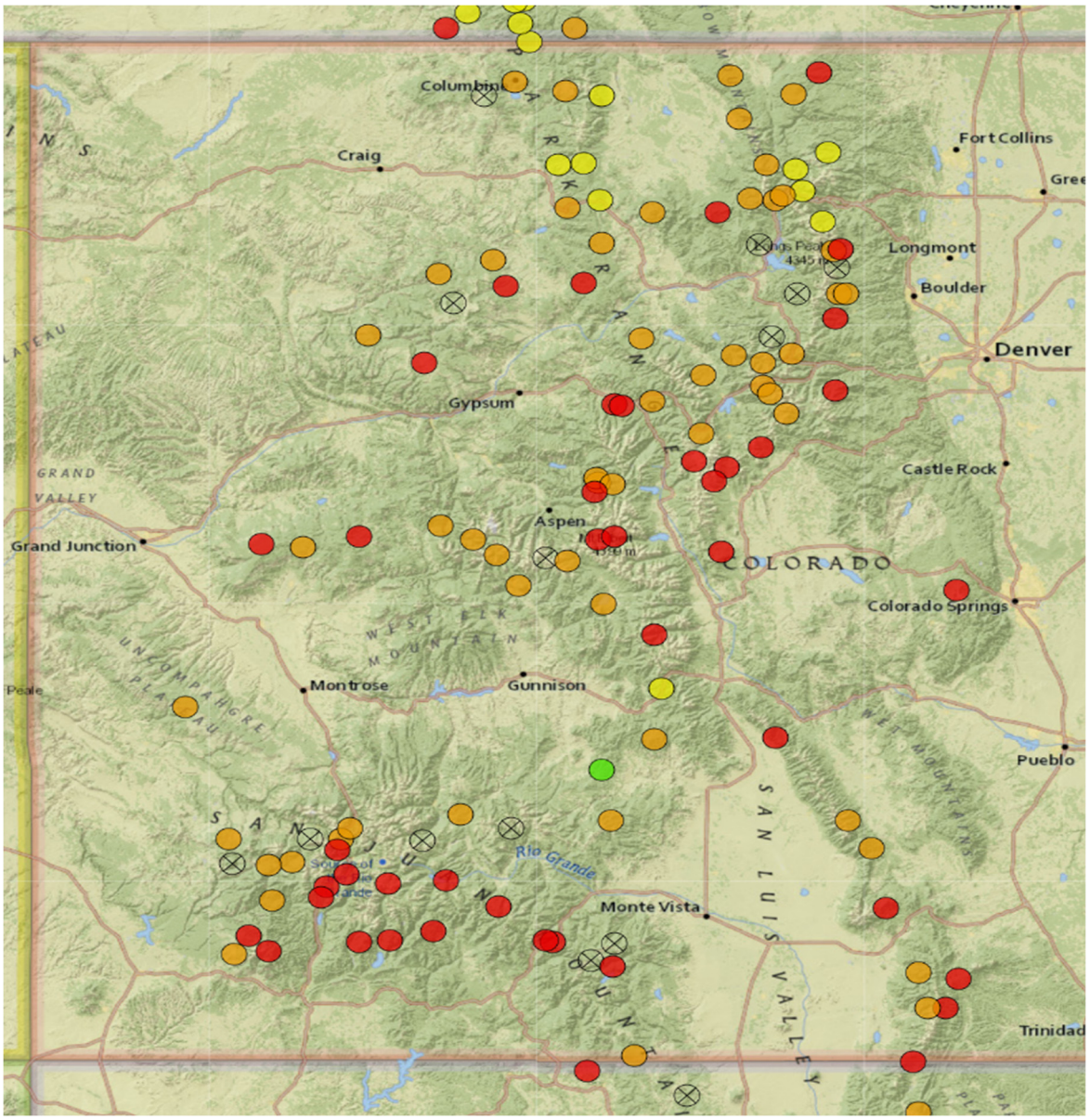

Figure B7. Colorado SNOTEL network characterized by Walker Water. The colors indicate late January levels as compared with average over several years.

The harmonic analysis and volcanic forcing approach used in Walker Water's snowpack forecasting system is grounded in published, peer-reviewed research. The underlying methodology has been validated across multiple independent physical systems, demonstrating that it captures genuine climate signals rather than fitting noise.

 doi:10.20944/preprints202604.0438.v1

Atmospheric Transmission

The volcanic impulse function framework was originally developed and validated using atmospheric transmission measurements collected at 880 nm wavelength from 1958 through 2018. A model incorporating 23 volcanic eruption impulses and 15 periodic functions achieves $R^2 = 0.94$, explaining 94% of the variance in atmospheric transparency over six decades. This independent validation demonstrates that the volcanic forcing parameterization captures real physical processes—stratospheric aerosol loading, residence time, and radiative effects—with high fidelity. The same mathematical framework, adapted for snowpack rather than optical transmission, is what produces the forecasts shown in this report.

Published Research

Walker Water's research has been published in peer-reviewed scientific journals. Key publications include work on harmonic analysis of Antarctic ice core records, demonstrating that periodic climate signals persist over geological timescales; analysis of CO_2 lag relationships during glacial cooling transitions; and investigation of climate interactions between water vapor and volcanic eruptions. These publications establish the theoretical and empirical basis for applying harmonic decomposition to climate-driven environmental systems.

Algorithm Characteristics

Several properties of the forecasting algorithm are relevant to understanding its performance and limitations. The system uses a greedy search with mathematical constraints to prevent overfitting—it systematically tests model configurations of varying complexity and selects the simplest model that achieves the highest prediction accuracy on held-out data. This reflects the well-established statistical principle that parsimonious models often extrapolate better than complex ones, even when the complex model fits the training data more closely.

The algorithm's fit quality is intentionally moderate (typical R^2 values of 0.15–0.35 against cross-validated data) after removal of a typical year's snowfall before fitting. This may seem low compared to models that report R^2 against their own training data, but it reflects honest out-of-sample performance. The system captures the periodic component of snowpack variation while accepting that weather-scale stochastic variation is inherently unpredictable at the one-year horizon. The useful output is not a precise SWE prediction but a graded forecast: whether the coming year will be above-normal, near-normal, or below-normal relative to the site's climatology.

Prediction Scope and Limitations

Walker Water's system predicts site-specific one-year-ahead peak SWE using periodic climate signals (ENSO, longer-period oscillations, volcanic forcing). It is designed to inform water managers on the probable reservoir fill under normal-to-moderate climate variation. The system does not predict and should not be relied upon to predict the following:

Catastrophic volcanic eruptions. Future eruptions cannot be predicted. The system incorporates the effects of past eruptions but has no capacity to anticipate future events. An eruption comparable to Pinatubo (1991) would produce a temporary forcing outside the model's scope.

Unprecedented drought or precipitation extremes. The harmonic model captures the frequency of ENSO oscillations but not the extreme amplitude of rare events. Seasons like 2010–2011, when an unusually strong La Niña produced record-low snowpack across much of the West, involve amplitudes that exceed the model's calibrated range.

Warm snow drought events. The 2017–2018 season demonstrated a failure mode where La Niña conditions coincided with anomalous warmth, causing precipitation to fall as rain rather than snow at many elevations. This reduced snowpack without reducing total precipitation—a mechanism the SWE-based harmonic model is not designed to capture.

 doi:10.20944/preprints202604.0438.v1

Single-storm or sub-seasonal events. The system operates at the annual timescale. It does not predict individual storms, atmospheric rivers, or the timing of melt onset within a season.

Within its designed scope, the system provides objective, reproducible forecasts that are validated against the full historical record at each site. The tier rating and pass rate offer a transparent measure of forecast reliability that water managers can incorporate into their planning frameworks alongside other data sources.

While anomalously strong or weak climate forcing events or extra-climate events cannot be predicted, when a water manager realizes that such an event is building, the given forecast for the year can be compared with a matching event in the prediction history of the specific site, for useful information on what to expect. Some sites are strongly affected by anomalous events while others show little change.

Appendix C: Configuration Search Order

Each phase tests the following configurations in order, stopping at early exit conditions:

- 1p/FNCA_0.40
- 2p/FNCA_0.20
- 2p/FNCA_0.10
- 2p/FNCA_0.05
- 2p/FNCA_0.02
- 3p/FNCA_0.20
- 3p/FNCA_0.10
- 3p/FNCA_0.05
- 4p/FNCA_0.20
- 4p/FNCA_0.10
- 4p/FNCA_0.05

Where np = number of harmonic periods and FNCA = overfitting constraint threshold. Lower FNCA = tighter orthogonality requirement. Configurations are tested from simplest (1p) to most complex (4p), and from tightest to loosest FNCA at each period count.

References

1. Higginbotham, J. (2026a). Climate, Water Vapor, and Volcanic Eruptions. Env Sci Climate Res, 4(1), 01–09. https://doi.org/10.33140/ESCR.04.01.01
2. Higginbotham, J. (2026b). Antarctic Ice Core Harmonic Analysis. Env Sci Climate Res, 4(1), 01–24. https://doi.org/10.33140/ESCR.04.01.04
3. Higginbotham, J. (2026c). CO_2 Lag as Glacial Cooling Initiates. Env Sci Climate Res, 4(1), 01–06. https://doi.org/10.33140/ESCR.04.01.05
4. Higginbotham, J. (2025). Planetary Orbits and Sea-Level. J Biomed Res Environ Sci, 6(4): 328–339. https://doi.org/10.37871/jbres2088
5. NRCS (2025). SNOTEL Network Data. Natural Resources Conservation Service, USDA. https://wcc.sc.egov.usda.gov/reportGenerator/
6. Barnston, A. G., & Livezey, R. E. (1987). Classification, seasonality and persistence of low-frequency atmospheric circulation patterns. Mon. Wea. Rev., 115, 1083–1126.
7. Dettinger, M. D., Cayan, D. R., Diaz, H. F., & Meko, D. M. (1998). North–south precipitation patterns in western North America on interannual-to-decadal timescales. J. Climate, 11, 3095–3111.
8. Mantua, N. J., Hare, S. R., Zhang, Y., Wallace, J. M., & Francis, R. C. (1997). A Pacific interdecadal climate oscillation with impacts on salmon production. Bull. Amer. Meteor. Soc., 78, 1069–1079.
9. Cayan, D. R. (1996). Interannual climate variability and snowpack in the western United States. J. Climate, 9, 928–948.
10. Trenberth, K. E. (1997). The definition of El Niño. Bull. Amer. Meteor. Soc., 78, 2771–2777.

 doi:10.20944/preprints202604.0438.v1

11. Mote, P. W., Hamlet, A. F., Clark, M. P., & Lettenmaier, D. P. (2005). Declining mountain snowpack in western North America. Bull. Amer. Meteor. Soc., 86, 39–49.
12. Dettinger, M. D. (2011). Climate change, atmospheric rivers, and floods in California—A multimodel analysis of storm frequency and magnitude changes. J. Amer. Water Resour. Assoc., 47, 514–523.
13. Higginbotham, J. (2025). Integrated Category Analysis, Walker Water LLC internal document.